International Journal of Industrial Chemistry (2018) 9:285–294
https://doi.org/10.1007/s40090-018-0158-z

RESEARCH

Electrochemically assisted photocatalytic removal of *m*-cresol using TiO_2 thin film-modified carbon sheet photoelectrode

Ebrahim Zarei[1]

Received: 22 September 2017 / Accepted: 11 October 2018 / Published online: 19 October 2018

Abstract

In this study, removal of *m*-cresol has been performed using photoeletrocatalysis technique at the surface of titanium dioxide (TiO_2) thin film-modified carbon sheet photoelectrode. A biased potential was applied across this photoelectrode illuminated by UV light to investigate the feasibility of an electrochemically assisted photocatalytic process in this degradation. For preparation of this photoelectrode, the photocatalytically active TiO_2 thin film was covered on the carbon sheet by dip coating technique using economically accessible TiO_2 powder (Degussa P25). It was found that the *m*-cresol could be degraded more efficiently by this photoelectrocatalytic process than the degradation obtained by photocatalytic oxidation or by electrochemical oxidation or alone. The effect of various parameters, such as *m*-cresol concentration, pH and applied potential on the photoelectrocatalytic degradation of *m*-cresol was studied and discussed.

Keywords *m*-Cresol · Degradation · Electrochemically assisted photocatalysis · TiO_2 thin film

Introduction

Traditional physical techniques, such as flocculation, adsorption on activated carbon and ultra-filtration may be employed efficiently to remove such recalcitrant pollutants. However, they are non-destructive, because they just transfer the dye compounds from water to another phase which would cause a secondary environmental pollution [1–6]. This has led to the requirement of regeneration of the adsorbent materials and post-treatment of solid wastes and both of them are expensive [7].

In the course of recent years, elective techniques as advanced oxidation processes (AOPs) for organic materials treatment have been studied [8–10], incorporating chemical oxidation with reagents for example: ozone, hydrogen peroxide, ozone/UV, hydrogen peroxide/UV and Fenton's reagent [hydrogen peroxide + Fe(II)]. A photocatalytic strategy for the oxidation of organic contaminants in wastewater by UV or solar irradiation and TiO_2 has additionally been investigated [11–16]. TiO_2 has very attractive properties such as environmentally friendly, low cost, low harmfulness and a wide band gap of 3.2 eV, which results in good stability and avoids photo-corrosion [17]. Generally, since TiO_2 is used as powder, which brings about a few disadvantages, for example, trouble in catalyst separation. This issue was expelled with catalyst immobilization on the solid surfaces. But, this technique intrinsically diminishes quantum efficiency because of the lessening of active surface area [18, 19]. Nevertheless, the high probability of hole–electron recombination in TiO_2 during the photocatalytic process has to be solved yet [20, 21].

The photoelectrochemical technology with external potential seems promising for research on photocatalytic degradation of organic pollutants, and many academic studies have been focused on this area [22–30]. Cresols are persistent compounds and are poisonous to a wide range of living beings. They may have adverse effects on ecosystems and additionally on human health, bringing about serious environmental contamination. *m*-Cresol is a methylated derivative of phenol and is a substance regarded as a priority contaminant by the United States Environmental Protection Agency (USEPA) [31, 32]. Cresols are utilized in the pharmaceutical and textile industries, and are produced as intermediates in the preparation of pesticides, to a great extent utilized in the formulation of antioxidants; they likewise have numerous uses in the fragrance industry [33]. This extensive range of industrial applications accounts for

✉ Ebrahim Zarei
e.zarei@cfu.ac.ir

[1] Department of Basic Sciences, Farhangian University, Tehran, Iran

the frequent presence of cresols as contaminants in industrial wastewater. The Ministry of Environment and Forest (MOEF), Government of India, has set a greatest concentration level of 1.0 mg L^{-1} of cresol in industrial effluent for safe discharge in the surface waters [34]. Thus, the removal of *m*-cresol has received extensive consideration using different techniques [35–38]. Notwithstanding, based on current information, application of photoelectrocatalytic methods for removal of *m*-cresol has not been reported.

In this study, the photoelectrocatalytic degradation of *m*-cresol using the TiO_2 thin film-modified carbon sheet photoelectrode was investigated. This electrode was provided by covering a carbon plate surface with a known quantity of the TiO_2 slurry. Furthermore, in this research, the effect of different factors (such as initial *m*-cresol concentration, pH value of solution, and bias potential used) was studied on degradation of *m*-cresol.

Experimental

Reagents

The solutions were prepared with deionized water. Orthophosphoric acid and its salts in the pH ranges 3.0–11.0 were applied to prepare buffer solutions. For fabricating the carbon paste electrode, paraffin (density 0.88 g cm^{-3}) and graphite powder (particle diameter 0.1 mm) from Fluka were utilized. The received *m*-cresol from Merck was used. Carbon electrodes were prepared from cutting a carbon sheet in the known size. TiO_2 powder with product name P-25, particle size 30 nm and surface area 50 m^2 g^{-1} was obtained from Degussa Corp. In TiO_2 powder, there is anatase form of TiO_2 as the significant portion compared to other forms.

Construction of the photoelectrode

Dip-coating strategy was employed for covering TiO_2 films from a TiO_2 suspension. To get ready of this suspension, a certain quantity of the Degussa P-25 powder was suspended in water (250 g L^{-1}) and sonicated for 30 min. After sonicating, a carbon sheet (3.0 × 3.0 cm^2) was dunked into TiO_2 suspension for 15 s and then lifted up and preheated at 90 °C for fabrication TiO_2 film. The technique from plunging to preheating was rehashed for six cycles. The TiO_2 loading corresponds to 6.6 mg of TiO_2 spread on an area of approximately 6.2 cm^2 of the carbon sheet. The uncovered area of the carbon sheet was used to make the electrical contact. Finally, the TiO_2-modified electrode was heated at 400 °C for 1 h. The TiO_2 thin film prepared stuck well to graphite surface and had sufficient stability in the pH limit 1–13.

Physical and photoelectrochemical characterization

The photoelectrocatalytic oxidation of *m*-cresol was performed in a single photoelectrochemical compartment which was constructed of a cylindrical quartz cell (3.0 cm diameter × 8.0 cm height with a 1.8 mm wall), a TiO_2-modified carbon sheet electrode as anode, a Pt rode serving as cathode, and an Ag/AgCl/KCl (3 M) serving as the reference electrode (Fig. 1). The reactor and the UV lamp were put in a black box to keep away from extraneous illumination. The photoreactor has three electrodes which were set in the center of the reactor in parallel and connected with the potentiostat (μ Autolab Type III). A carbon paste electrode (CPE) was utilized as a working electrode for electrochemical examination of *m*-cresol concentration variations in the different processes such as photoelectrocatalysis by measurements of the peak current (I_P) decay at the peak potential (E_P) oxidation of *m*-cresol in its differential pulse voltammograms over various times. The scan rate for recording DPVs was 10 mV s^{-1}. The photoactive surface of the anode (TiO_2) was illuminated by a 4 W medium pressure mercury lamp with a power intensity of 0.4 mW cm^{-2} as UV light source. Scanning electron microscopy (SEM) (Philips Corp., XL30 model) was used for seeing of the surface morphology of the TiO_2-modified carbon electrode. Measurements of pH were made with a Denver Instrument Model 827 pH meter equipped with a Metrohm glass electrode. Zeta potential of the TiO_2 was measured using a Zeta potential meter (Stabino, Particle Mertix Company, Germany).

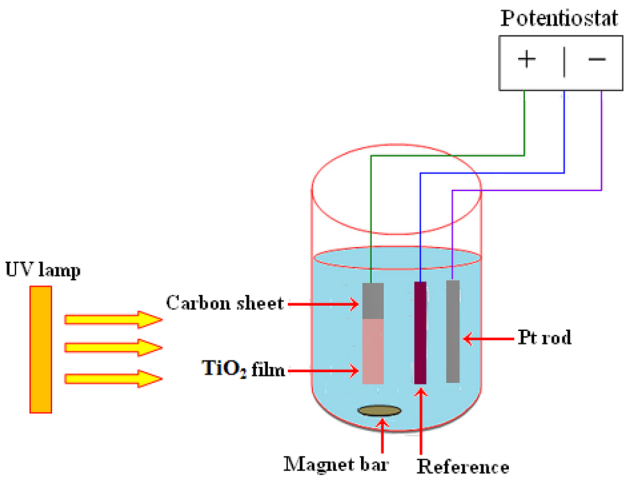

Fig. 1 Schematic diagram of the photoreactor system

Results and discussion

Surface morphology of the photoelectrode

The TiO_2-modified photoelectrode surface was studied utilizing SEM. Figure 2 indicates typically the top of SEM pictures of the unmodified (A) and TiO_2-modified (B) carbon electrodes. It can be shown from the micrograph that spherical TiO_2 particles were distributed uniformly on the surface of carbon, and that the mean size is nearly equal to that of the original Degussa P25 TiO_2. The cross-sectional image of TiO_2 film (Fig. 2c) clearly shows three different layers: (1) a porous transparent TiO_2 layer ~ 4.3 µm, and (2) a scattered TiO_2 layer ~ 1.0 µm.

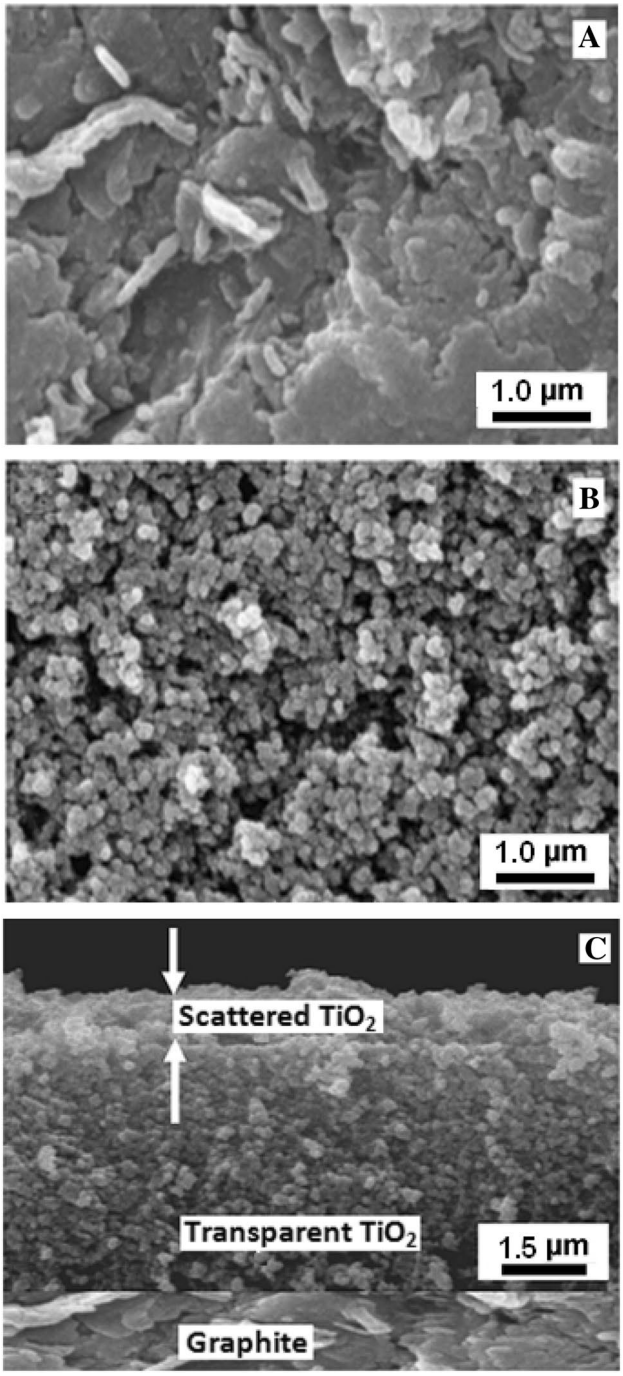

Fig. 2 The top of SEM micrographs of **a** unmodified and **b** TiO_2-modified carbon sheet electrodes. **c** A cross-sectional photograph of TiO_2 thin film on the carbon sheet

Photoelectrochemical properties of the photoelectrode

The mechanisms underlying the heterogenous photocatalysis employing the semiconductor TiO_2 catalyst have been intensively reported in many papers [39]. The key reactions involved in the photocatalysis are listed in Table 1. Upon irradiation of TiO_2 with light energy equivalent to or greater than its band gap energy (anatase ~ 3.2 eV), the electron is excited from valence band (VB) to the conduction band (CB) (Eq. 1). Figure 3a(1) depicts the mechanism of the electron–hole pair formation when the TiO_2 particle is irradiated with light of adequate energy. The light wavelength for such photon energy usually corresponds to $\lambda < 400$ nm. Owing to the reaction between the photogenerated vacancy and adsorbed water, a heterogeneous hydroxyl radical is generated and then this radical can be straightforwardly oxidized by the hole or by $^{\cdot}OH$ formed from Eq. (2). Likewise, the photoinjected electron can create other oxidizers such as $O_2^{\cdot-}$, $HO_2^{\cdot}$ and H_2O_2 with less strength and more $^{\cdot}OH$ based on Eqs. (3–6). The recombination of electrons ascended to the valence band either with unreacted holes or with adsorbed hydroxyl radicals which is the notable obstacle of photocatalysis as observed in Fig. 3a(2) and Eqs. (7, 8).

The application of an anodic bias to a TiO_2-modified photoelectrode further provides a potential gradient within the film to drive away the photogenerated holes and electrons in different directions efficiently. The photogenerated holes could oxidize the organic mixtures at the anode surface [Fig. 3a(3)], while the photogenerated electrons were transferred to the receiver at the metallic cathode through

Table 1 Some basic reactions involved in the photocatalysis process

Reaction equation	Number
$TiO_2 + h\nu \rightarrow e^-_{CB} + h^+_{VB}$	(1)
$h^+_{VB} + H_2O \rightarrow {}^{\cdot}OH + H^+$	(2)
$e^-_{CB} + O_2 \rightarrow O_2^{\cdot-}$	(3)
$O_2^{\cdot-} + H^+ \rightarrow HO_2^{\cdot}$	(4)
$2HO_2^{\cdot} \rightarrow H_2O_2 + O_2$	(5)
$H_2O_2 + O_2^{\cdot-} \rightarrow {}^{\cdot}OH + OH^- + O_2$	(6)
$e^-_{CB} + h^+_{VB} \rightarrow TiO_2 + \text{heat}$	(7)
$e^-_{CB} + {}^{\cdot}OH \rightarrow OH^-$	(8)

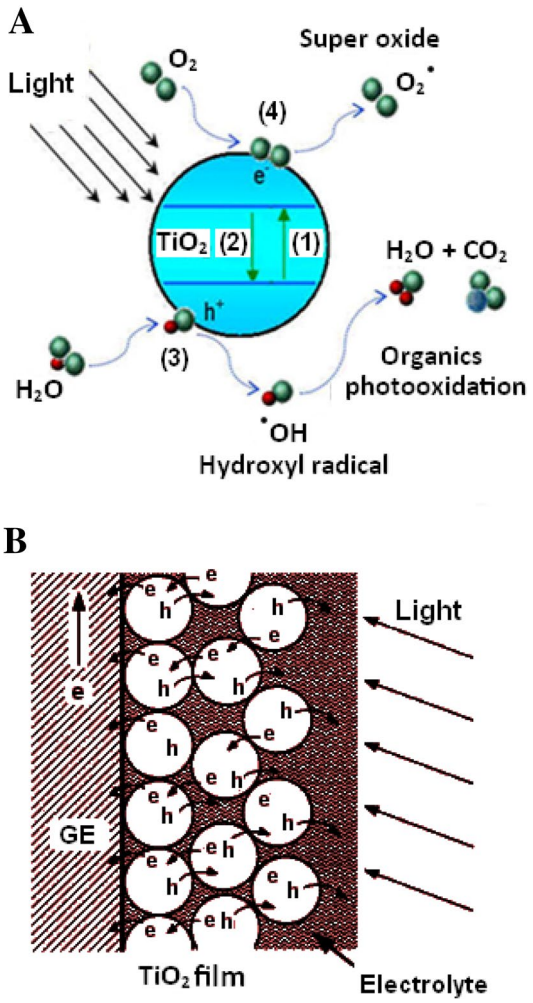

Fig. 3 Schematic photoexcitation of a semiconductor particle (**a**) and separation of electron–hole using an anodic voltage (**b**)

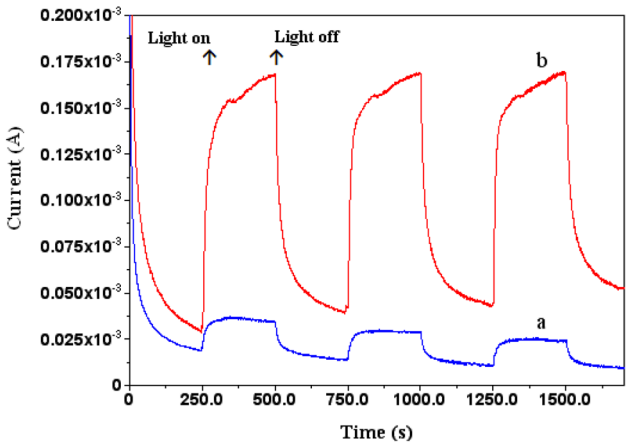

Fig. 4 Photocurrent–time curves of the TiO_2-modified carbon sheet electrode for several on–off cycles of radiation at an applied potential of 0.45 V in phosphate buffer solution (pH 7.0) in the a absence of *m*-cresol and b presence of 400.0 mg L^{-1} *m*-cresol

the outside electrical circuit [Fig. 3a(4)]. As mentioned in Fig. 3b, thin semiconductor special films obtained from especial suspensions contains small particles which are in near contact with each other and are capable of showing photoelectrochemical characteristics similar to polycrystalline semiconductor films.

Hydrodynamic amperometry was utilized in buffer solution in the presence and absence of *m*-cresol solution under UV light to investigate photoelectrochemical answer of the TiO_2-modified photoelectrode (Fig. 4). As appeared in Fig. 4, the ascent and fall of the photocurrent reacted well to the illumination being turned on and off. The photocurrent comes on expeditiously after the illumination, and afterward the photocurrent achieves a consistent state. This pattern of photocurrent can be highly reproduced for several on–off cycles of radiation. A certain increase seen in the photocurrent under illumination shows that photogenerated electrons on the TiO_2-modified photoelectrode can be adequately directed to the auxiliary electrode utilizing applied positive potential, which would be crucial for banning of charge recombination. The presence of *m*-cresol in buffer solution gives a significantly easier mechanism for the exchange of the photogenerated holes in the TiO_2-modified photoelectrode over the film/electrolyte interface against either adsorbed water molecules or hydroxyl groups. As a result, the higher photocurrent is created in the presence of *m*-cresol.

Furthermore, to more assess the photoelectrochemical activity of the TiO_2-modified photoelectrode and to make sure its ability to oxidize *m*-cresol by photoelectrocatalysis, cyclic voltammetry tests in the dark and under UV light illumination were carried out both with and without *m*-cresol (Fig. 5). As can be observed in Fig. 5, the electrochemical oxidation current value of the TiO_2-modified photoelectrode in the presence of *m*-cresol in the dark environment and under irradiation is varying (curves c and d). This demonstrates that *m*-cresol as a hole scavenger by obtaining holes could be viably oxidized and as a result would be effective positively to electron–hole separation.

Comparison of different methods for *m*-cresol removal

Experiments on photoelectrocatalytic, photocatalytic, electrochemical and direct photolytic degradation of *m*-cresol were conducted to compare *m*-cresol degradation efficiencies among four individual processes (Fig. 6). All experiments were carried out in phosphate buffer solution (pH 7.0) containing initial *m*-cresol concentration 7.0 mg L^{-1}. Also, about photoelectrocatalytic and electrochemical degradation processes, the investigations were performed at the surface

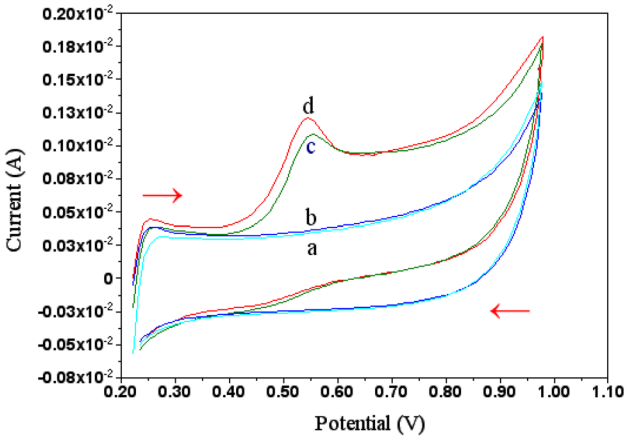

Fig. 5 Cyclic voltammograms of the TiO_2-modified carbon sheet electrode in phosphate buffer solution (pH 7.0) a under dark conditions and b under UV irradiation, c under dark conditions containing 400.0 mg L^{-1} *m*-cresol and d under UV irradiation containing 400.0 mg L^{-1} *m*-cresol

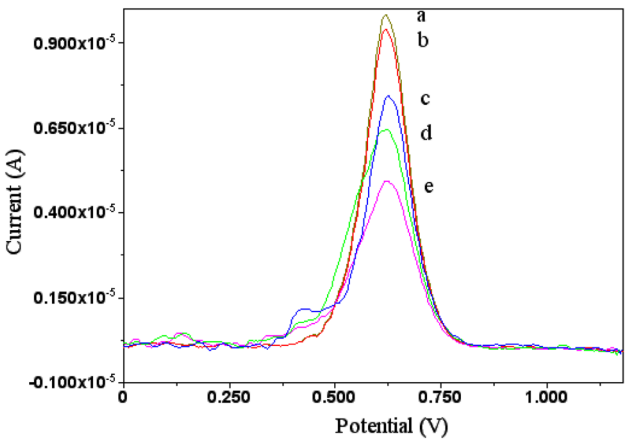

Fig. 6 Differential pulse voltammograms of 7.0 mg L^{-1} *m*-cresol at the TiO_2-modified carbon sheet electrode surface before (a) and after (b) electrochemical, c direct photolytic, d photocatalytic and e photoelectrocatalytic degradation processes, in 0.1 M phosphate buffer solution (pH 7.0) and $E = 0.45$ V vs Ag/AgCl/KCl (3 M)

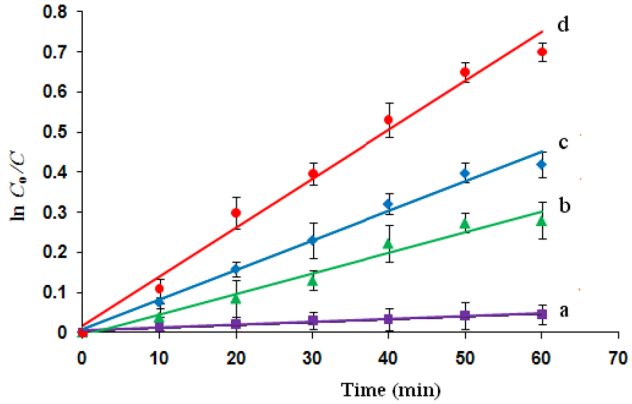

Fig. 7 Plot of $\ln C_o/C$ as a function of time for degradation of *m*-cresol using a photoelectrocatalysis, b photocatalysis, c direct photolysis and d electrochemical oxidation methods (calculated based on the data of Fig. 6)

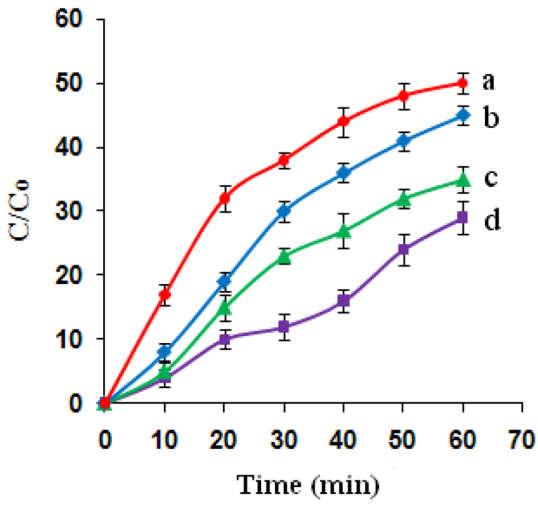

Fig. 8 Effect of different initial *m*-cresol concentration on *m*-cresol degradation: a 5.0, b 7.0, c 9.0 and d 11.0 mg L^{-1} on photoelectrocatalytic degradation of *m*-cresol in phosphate buffer solution (pH 3.0) on a TiO_2-modified carbon sheet electrode biased at $E = 0.45$ V

of TiO_2-modified photoelectrode biased at $E = 0.45$ V. In Fig. 6 and other Figs. 7, 8 and 9, the relative concentration of *m*-cresol, C/C_o, was obtained by evaluating the ratio of *m*-cresol concentration C at time t and the initial *m*-cresol concentration C_o in the solution, at $t = 0$. It is easy to see that only 4.5% *m*-cresol was removed by electrochemical oxidation within 60 min, which indicates that the direct photolysis and photocatalysis processes played important roles in the removal of *m*-cresol. The removal efficiencies obtained by the two techniques were 28 and 42%, respectively, while the removal efficiency by photoelectrocatalysis was higher, to 70%, inside the similar time. As can be seen, the experimental results approved that the removal rate of *m*-cresol in the photoelectrocatalytic oxidation was more than that of the photocatalytic, direct photolytic and electrochemical oxidation.

Figure 7 indicates differential pulse voltammograms of *m*-cresol in the various times for photoelectrocatalytic process with scan rate 10 mV s^{-1} for instance. For kinetic description of the photocatalytic and photoelectrocatalytic reactions, the Langmuir–Hinshelwood kinetic model formula has often been utilized. The experimental results can well fit the first-ordered reaction model equation, $\ln(C_o/C) = f(t) = kt$ (k is rate constant) (Fig. 7). Utilizing the slope of the curve, the corresponding reaction rate constant, k, can be calculated for evaluation of the degradation efficiency of *m*-cresol in the electrochemically

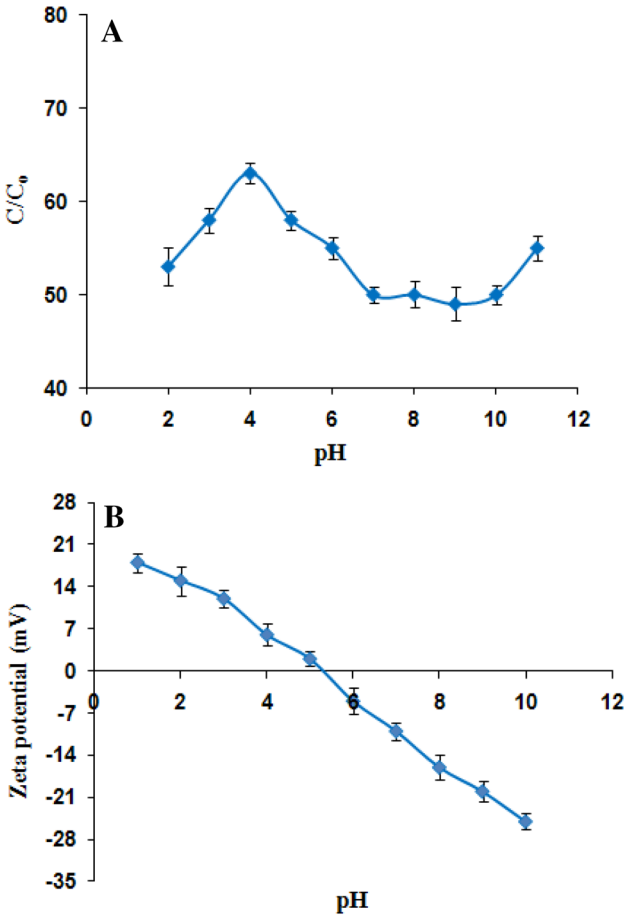

Fig. 9 **a** Photoelectrocatalytic removal of *m*-cresol as affected by pH on photoelectrocatalytic degradation of *m*-cresol in solution containing initial *m*-cresol concentration 5.0 mg L^{-1} on a TiO_2-modified carbon sheet electrode biased at $E=0.45$ V. **b** The Plot of zeta potential for TiO_2 nanoparticles suspended in phosphate buffers as a function of the pH of the suspension

Table 2 Rate constants (k) and electrical energy per order (E_{Eo}) compared PEC degradation of *m*-cresol with PC, DP and EC removal processes

Process	K (MIN^{-1})	Correlation coefficient (R)	E_{Eo} (kW h m^3 $order^{-1}$)
PEC	0.0122	0. 9853	630
PC	0.0074	0.9882	1038
DP	0.0052	0.9724	1477
EC	0.0007	0.9647	10,971

assisted photocatalysis, photocatalysis, direct photolysis and electrochemical oxidation processes. The experimental results summarized in Table 2 demonstrated that the reaction rate of *m*-cresol degradation in the electrochemically assisted photocatalysis process was faster than that of photocatalysis, direct photolysis and electrochemical oxidation.

There are various important factors in choosing a waste-treatment technology, inducing economics, economy of scale, regulations, effluent quality aims, operation (maintenance, control, safety) and robustness (flexibility to change/upsets). Despite the fact that these factors are necessary, financial aspects are frequently paramount. Since photodegradation of aqueous organic pollutant is an electric energy-intensive process, and electric energy can represent a noteworthy portion of the operating costs, simple figures-of-merit based on electric energy consumption can be very useful and informative. Recently, the international union of pure and applied chemistry (IUPAC) has proposed two figures-of-merits for advanced oxidation processes (AOPs) on the utilization of electrical energy. In the zero-order range, the appropriate figure-of-merit is the electrical energy per mass (E_{Em}) defined as the kW h of electrical energy required for degradation of one kg of the pollutant [40]. In the case of low pollutant concentrations, which applies here, the appropriate figure-of-merit is the electrical energy per order (E_{Eo}), defined as the number of kW h of electrical energy required to reduce the concentration of a pollutant by 1 order of magnitude (90%) in 1 m^3 of contaminated water. The E_{Eo} (kW h m^3 $order^{-1}$) can be determined from the following equations:

$$E_{Eo} = P \times t \times 60 \times 1000/V \times \ln\left(C_o/C\right), \tag{9}$$

$$\ln\left(C_o/C\right) = k \times t, \tag{10}$$

where P is the rated power (kW) of the AOP system, t is the illumination time (min), V is the volume (L) of the water in the reactor, C_o and C are the initial and final pollutant concentrations and k is the pseudo-first-order rate constant (min^{-1}) for the decay of the pollutant concentration [41, 42]. From Eqs. (9) and (10), E_{Eo} can be written as follows:

$$E_{Eo} = (38.4 \times P)/(V \times k). \tag{11}$$

The calculated E_{Eo} values for photoelectrocatalytic, photocatalytic, electrochemical and direct photolytic degradation of *m*-cresol are shown in Table 2. As it is clear, the efficiency of photoelectrocatalysis process is higher than other degradation processes.

The supposed degradation reactions paths are shown in Scheme 1 [43]. Based on this scheme, the photoproducts of *m*-cresol in aqueous solution were 3-hydroxybenzaldehyde(**1**), 2-methylben-zene-1,4-diol(**2**), 4-methylbenzene-1,2-diol(**3**), 3-methylben-zene-1,2-diol(**4**), 2,2′-dimethylbiphenyl-4,4′-diol(**5**), 2′,4-di-methylbiphenyl-2,4′-diol(**6**), 4,4′-dimethylbiphenyl-2,2′-diol (**7**), 2′,6-dimethylbiphenyl-2,4′-diol(**8**), 3-methyl-4-(*m*-toly-loxy)phenol(**9**).

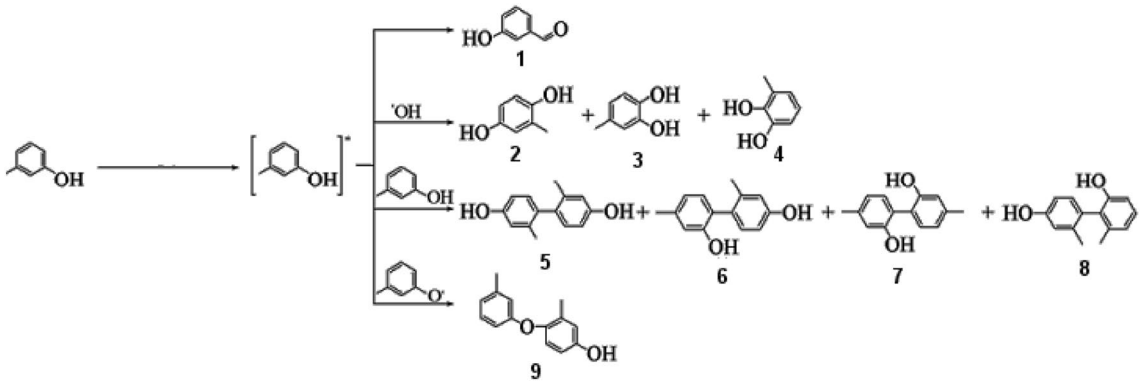

Scheme 1 Proposed degradation of *m*-cresol reactions and suggested products

Effect of initial *m*-cresol concentration

Figure 8 demonstrates the profiles of photoelectrochemical degradation of *m*-cresol at its different initial concentrations. The experiments were performed in phosphate buffer solution (pH 7.0) containing 5.0, 7.0, 9.0 and 11.0 mg L^{-1} *m*-cresol on a TiO_2-modified photoelectrode biased at $E = 0.45$ V vs. reference electrode. It can be seen that the amount of the photoelectrocatalytic degradation of *m*-cresol increased but the reaction rate diminished sharply with the increase of the initial concentration of *m*-cresol. Since the photo-assisted electrocatalytic oxidation occurred on the catalyst surface, not in the bulk of the solution [44, 45], the reduction in *m*-cresol degradation rate at higher initial *m*-cresol concentrations can be explained by the fact that at higher *m*-cresol concentrations, the light intensity reaching the TiO_2 film surface is reduced due to the lower transparency of the solution.

Effect of pH amount

The pH value is an important factor in the photocatalytic and photoelectrocatalytic removal processes, because the pH value of the solution will alter the present configuration of degraded types and surface charges of catalysts. As a result, the species of the reaction mixtures and its adsorption balance on the TiO_2 depend on the pH values of reaction solution. Moreover, it should be pointed out that the other parameters, e.g., the adsorption size of the active species similar to elemental oxygen and decreased potential of TiO_2 valence band changes [46], affect the photoelectrocatalysis process according to the pH value. The effect of pH on the degradation rate of *m*-cresol is presented in Fig. 9a (initial *m*-cresol concentration 5.0 mg L^{-1} over 1 h illumination). For this aim, the effect of pH value was investigated through the experiments conducted with 5.0 mg L^{-1} *m*-cresol in buffer solutions with pH 3.0–11.0 on the TiO_2-modified photoelectrode biased at $E = 0.45$ V. One can observe that the degradation rate is highest at pH 4.0. Also, we can easily see that the amount of *m*-cresol degraded decreases sharply to pH 7.0 but it is almost constant to pH 10.0 and then increases after that at pH 11.0.

Figure 9b shows the results of measuring the zeta potential for suspended TiO_2 particles as function of the pH of the suspension. The pH of the iso-electric point for TiO_2 was found to be almost 5.2. Hydroxyl groups on TiO_2 surface under various pH amount conditions, undergo the following reactions [47]:

$$\text{pH} < \text{PZC: TiOH} + \text{H}^+ \rightleftarrows \text{TiOH}_2^+, \tag{12}$$

$$\text{pH} > \text{PZC: TiOH} + \text{OH}^- \rightleftarrows \text{TiO}^- + \text{H}_2\text{O}. \tag{13}$$

The catalyst surface is positively charged while at pH value above just about 6.0, henceforth, at more acidic pH, it is negatively charged [48]. Also, since *m*-cresol is as weak organic acid in water, therefore, depending on the pH value in the solution, *m*-cresol might be exhibited in various structures. In this way, the adsorption amount of *m*-cresol at the surface TiO_2 most likely as the initial step in the process of photoelectrocatalysis and subsequently photoelcectrocatalytic degradation efficiency of *m*-cresol is related to the initial pH value of the solution. pH has doublet effect in reaction, one is pH effect in adsorption of substrate molecules and second is pH effect in the OH^- and $OH^{\cdot}$ concentration that affected degradation performance resulting from reaction of holes with H_2O. Therefore, in some cases, these two effects are alien and reversely affected degradation performances. In these cases, adsorption of substrate molecules at the surface of electrode is more effective than $OH^{\cdot}$ concentration. For photoelectrocatalytic and photocatalytic degradation of compounds, it is necessary that compounds are absorbed at the surface of TiO_2. Studies showed that pH 4.0 was optimum pH for photoelectrocatalytic degradation of *m*-cresol (Fig. 9). At low pH values, *m*-cresol molecules presented in the neutral form might be effectively adsorbed onto the surface of TiO_2 with positive charges. In pH > 8,

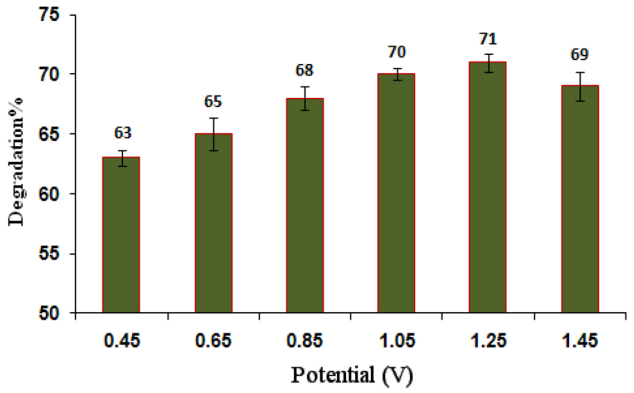

Fig. 10 Influence of different applied potentials on degradation of *m*-cresol in phosphate buffer solution (pH 4.0) containing initial *m*-cresol concentration 5.0 mg L^{-1} with time experiment 60 min

the surface containing negative charge steadily is shaped onto TiO_2 and due to the repulsion effect between the TiO_2 surface and the ionized *m*-cresol with negative charge at high pH, adsorption of *m*-cresol at the surface TiO_2 and accordingly its degradation turn out to be substantially more difficult than that at low pH values. Therefore, it can be expected that more acidic pH amounts would be desirable for the photoelectrocatalytic degradation of *m*-cresol. At pH 11.0, *m*-cresol oxidation is being easier due to the presence of large amounts of hydroxyl radicals with strong oxidizing capacity [49].

Effect of bias potential

It is obvious that the degradation rate of expanded increased significantly as the applied cell voltage increased. Applying a potential gradient over the titania film resulted in an electric field, which keeps photogenerated charges separated and forced the photogenerated holes and electrons to move in inverse directions. Therefore, bias potential is a key element that affects photoelectrocatalytic removal efficiency. Experiments were conducted in phosphate buffer solution (pH 4.0) containing *m*-cresol concentration 3.8 mg L^{-1} over time experiment 60 min using five levels of bias potential, 0.45, 0.65, 0.85, 1.05, 1.25 and 1.45 V (Fig. 10). These results obviously exhibit that the degradation rate increases as a function of applied potential up to $E = 1.25$ V. These outcomes suggest that the production and segregation of electron–hole pairs are accelerated under higher voltage situations. The majority of the photogenerated electrons were evacuated either by the electric field or by reaction with dissolved oxygen. Degradation prompted with further increase in potential. The reason of this subject might be the oxidation of more water by photogenerated holes [45]. As a result, potential 1.25 V was chosen as the best potential for investigating the degradation of *m*-cresol.

Conclusion

In this work, TiO_2-modified carbon plate photoelectrode was used as an appropriate electrode for degradation of *m*-cresol. Results demonstrated that photo-assisted electrocatalysis degradation of *m*-cresol was more compelling than different procedures, for example, direct photolytic, electrochemical and photocatalytic removal. Likewise, it was observed that PEC degradation of *m*-cresol at the surface of the TiO_2-modified photoelectrode significantly was dependent on buffer pH, initial *m*-cresol concentration and bias potential applied through electrode. The improvement of *m*-cresol removal in the photoelectrocatalysis process was credited to photoinduced electron and hole separation by the bias potential and in view of acquired results, direct electrochemical degradation was not involved. Such a helpful aspect of electrochemically assisted photocatalysis can apply its use in photocatalytic reactors with immobilized semiconductor particles.

References

1. Ma L, Sun C, Ren J, Wei H, Liu P (2014) Efficient electrochemical incineration of phenol on activated carbon fiber as a new type of particulates. Russ J Electrochem 50:569–578
2. Tang Y, Li H, Zhu H, Tian R, Gao X (2016) Impact of electric field on Hofmeister effects in aggregation of negatively charged colloidal minerals. J Chem Sci 128:141–151
3. Sen BK, Deshmukh DK, Deb MK, Verma D, Pal J (2014) Removal of phenolic ompounds from aqueous phase by adsorption onto polymer supported iron nanoparticles. Bull Environ Contam Toxicol 93:549–554
4. Ossman ME, Mansour MS (2013) Removal of Cd(II) ion from wastewater by adsorption onto treated old newspaper: kinetic modeling and isotherm studies. Int J Ind Chem 4:13
5. Chow CWK, Leeuwen JA, Fabris R, Drikas M (2009) Optimised coagulation using aluminium sulfate for the removal of dissolved organic carbon. Desalination 245:120–134
6. Lachheb H, Puzenat E, Houas A, Ksibi M, Elaloui E, Guillard C, Herrmann JM (2002) Photocatalytic degradation of various types of dyes (alizarin s, crocein orange g, methyl red, congo red, methylene blue) in water by UV-irradiated titania. Appl Catal B Environ 39:75–90
7. Cooper P (1993) Removing colour from dyehouse waste waters-a critical review of technology available. J Soc Dyers Colour 109:97–100
8. Tabaï A, Bechiri O, Abbessi M (2017) Degradation of organic dye using a new homogeneous Fenton-like system based on hydrogen peroxide and a recyclable Dawson-type heteropolyanion. Int J Ind Chem 8:83–89

9. Rao ChV, Giri AS, Goud VV, Golder AK (2016) Studies on pH-dependent color variation and decomposition mechanism of brilliant green dye in fenton reaction. Int J Ind Chem 7:71–80
10. Kasiri MB, Modirshahla N, Mansouri H (2013) Decolorization of organic dye solution by ozonation; optimization with response surface methodology. Int J Ind Chem 4:3
11. Carneiro PA, Osugi ME, Sene JJ, Andersonb MA, Zanonia MV (2004) Evaluation of color removal and degradation of a reactive textile azo dye on nanoporous TiO_2 thin-film electrodes. Electrochim Acta 49:3807–3820
12. Garcia JC, Oliveira JL, Silva AEC, Oliveira CC, Nozaki J, de Souza NE (2007) Comparative study of the degradation of real textile effluents by photocatalytic reactions involving UV/TiO_2/H_2O_2 and UV/Fe^{2+}/H_2O_2 systems. J Hazard Mater 147:105–110
13. Shokri A, Mahanpoor K (2017) Degradation of ortho-toluidine from aqueous solution by the TiO_2/O_3 process. Int J Ind Chem 8:101–108
14. Hauf MA, Ashraf S, Alhadrami SN (2005) Photolytic oxidation of coomassie brilliant blue with H_2O_2. Dyes Pigments 66:197–200
15. Yu D, Cai R, Liu Z (2004) Studies on the photodegradation of rhodamine dyes on nanometer-sized zinc oxide. Spectrochim Acta A Mol Biomol Spectrosc 60:1617–1624
16. Li Y, Yuan J, Gao S, Li L, Jiao S, Jin Y, Li H, Wang J, Yu Q, Zhang Y (2017) A facile route to synthesis of double-sided TiO_2 nanotube arrays for photocatalytic activity. J Mater Sci Mater Electron 28:468–473
17. Peralta-Hernándeza JM, Meas-Vonga Y, Rodrígueza FJ, Chapmana TW, Maldonadob MI, Godíneza LA (2006) In situ electrochemical and photoelectrochemical generation of the fenton reagent: a potentially important new water treatment technology. Water Res 40:1754–1762
18. Byrne JA, Eggins BR, Brown NMD, McKinney B, Rouse M (1998) Immobilisation of TiO_2 powder for the treatment of polluted water. Appl Catal B Environ 17:25–36
19. Leng WH, Zhang Z, Zhang JQ (2003) Photoelectrocatalytic degradation of aniline over rutile TiO2/Ti electrode thermally formed at 600 °C. J Mol Catal A Chem 206:239–252
20. Baram N, Starosvetsky D, Starosvetsky J, Epshtein M, Armon R, Ein-Eli Y (2009) Enhanced inactivation of *E. coli* bacteria using immobilized porous TiO_2 photoelectrocatalysis. Electrochim Acta 54:3381–3386
21. Chen XB, Mao SS (2007) Titanium dioxide nanomaterials: synthesis, properties, modifications, and applications. Chem Rev 107:2891–2959
22. Zarei E, Ojani R (2017) Fundamentals and some applications of photoelectrocatalysis and effective factors on its efficiency: a review. J Solid State Electrochem 21:305–336
23. Tian M, Adams B, Wen J, Asmussen RM, Chen A (2009) Photoelectrochemical oxidation of salicylic acid and salicylaldehyde on titanium dioxide nanotube arrays. Electrochim Acta 54:3799–3805
24. Sirés I, Brillas E, Oturan MA, Rodrigo MA, Panizza M (2014) Electrochemical advanced oxidation processes: today and tomorrow. a review. Environ Sci Pollut Res 21:8336–8367
25. Ojani R, Raoof JB, Khanmohammadi A, Zarei E (2012) Photoelectrocatalytic degradation of 3-nitrophenol at surface of Ti/TiO_2 electrode. J Solid State Electrochem 17:63–68
26. Orudzhev FF, Aliev ZM, Gasanova FG, Isaev AB, Shabanov NS (2015) Photoelectrocatalytic oxidation of phenol on TiO_2 nanotubes under oxygen pressure. Russ J Electrochem 51:1108–1114
27. Oturan MA (2014) Electrochemical advanced oxidation technologies for removal of organic pollutants from water. Environ Sci Pollut Res 21:8333–8335
28. Hou Y, Li X-Y, Zhao Q-D, Quan X, Chen G-H (2010) Electrochemical method for synthesis of a $ZnFe_2O_4$/TiO_2 composite nanotube array modified electrode with enhanced photoelectrochemical activity. Adv Funct Mater 20:2165–2174
29. Hou Y, Li X, Zou X, Quan X, Chen G (2009) Photoeletrocatalytic activity of a Cu_2O-loaded self-organized highly oriented TiO_2 nanotube array electrode for 4-chlorophenol degradation. Environ Sci Technol 43:858–863
30. Hou Y, Li X, Zhao Q, Chen G, Raston CL (2012) Role of hydroxyl radicals and mechanism of Escherichia coli inactivation on Ag/AgBr/TiO_2 nanotube array electrode under visible light irradiation. Environ Sci Technol 46:4042–4050
31. Yan J, Jianping W, Jing B, Daoquan W, Zongding H (2006) Phenol biodegradation by the yeast *Candida tropicalis* in the presence of *m*-cresol. Biochem Eng J 29:227–234
32. Bai J, Wen JP, Li HM, Jiang Y (2007) Kinetic modeling of growth and biodegradation of phenol and *m*-cresol using *Alcaligenes faecalis*. Process Biochem 42:510–517
33. Agency for Toxic Substances and Disease Registry (ATSDR) (2008) Toxicological profile for cresols., US Department of Health and Human Services, Public Health Services, Division of Toxicology and Environmental Medicine/Applied Toxicology Branch 1600 Clifton Road NE Mailstop F-32 Atlanta, Georgia 30333
34. Singh RK, Kumar S, Kumar S, Kumar A (2008) Biodegradation kinetic studies for the removal of *p*-cresol from wastewater using *Gliomastic indicus* MTCC 3869. Biochem Eng J 40:293–303
35. Chu Y, Zhang D, Liu L, Qian Y, Li L (2013) Electrochemical degradation of *m*-cresol using porous carbon-nanotube-containing cathode and Ti/SnO_2–Sb_2O_5–IrO_2 anode: kinetics, byproducts and biodegradability. J Hazard Mater 252–253:306–312
36. Abdollahi Y, Zakaria A, Sairi NA (2014) Degradation of high level *m*-cresol by zinc oxide as photocatalyst. Soil Water 42:1292–1297
37. Hopper DJ, Taylor DG (1975) Pathways for the degradation of *m*-cresol and *p*-cresol by *Pseudomonas putida*. J Bacteriol 122:1–6
38. Saravanan P, Pakshirajan K, Saha P (2009) Batch growth kinetics of an indigenous mixed microbial culture utilizing *m*-cresol as the sole carbon source. J Hazard Mater 162:476–481
39. Gu D, Wang Y, Li Z, Liu Y, Wang B, Wu H (2016) UV-light aided photoelectrochemical synthesis of Au/TiO_2 NTs for photoelectrocatalytic degradation of HPAM. RSC Adv 6:63711–63716
40. Natarajan TS, Natarajan K, Bajaj HC, Tayade RJ (2011) Energy efficient UV-LED source and TiO_2 nanotube array-based reactor for photocatalytic application. Ind Eng Chem Res 50:7753–7762
41. Stephen C, Stefan MI, Bolton JR, Safarzadeh-Amiri A (2000) UV/H_2O_2 treatment of methyl tert-butyl ether in contaminated waters. Environ Sci Technol 34:659–662
42. Bolton JR, Bircger KG, Tumas W, Tolman CA (2001) Figure-of merit for the technical development and application of advanced oxidation technologies for both electric- and solar-derived systems. Pure Appl Chem 73:627–637
43. Fei PG, Hong-hai X, Xiao-jian T, Chun-li K, Lin-lin L, Zhe L (2012) Comparison of photochemical reactions of *m*-cresol in aqueous solution and in ice. Chem Res Chin Univ 28:47–52
44. Lewerenz HJ, Heine C, Skorupska K, Szabo N, Hannappel T, Vo-Dinh T, Campbell SA, Klemm HW, Munoz AG (2010) Photoelectrocatalysis: principles, nanoemitter applications and routes to bio-inspired systems. Energy Environ Sci 3:748–760
45. Hitchman ML, Tian F (2002) Studies of TiO_2 thin films prepared by chemical vapour deposition for photocatalytic and photoelectrocatalytic degradation of 4-chlorophenol. J Electroanal Chem 538–539:165–172
46. Quan X, Ruan X, Zhao H, Chen S, Zhao Y (2007) Photoelectrocatalytic degradation of pentachlorophenol in aqueous solution using a TiO_2 nanotube film electrode. Environm Pollut 147:409–414
47. Nohara K, Hidaka H, Pelizzetti E, Serpone N (1997) Processes of formation of NH_4^+ and NO_3^- ions during the photocatalyzed oxidation of N-containing compounds at the titania/water interface. J Photochem Photobiol A Chem 102:265–272
48. Zhang W, An T, Xiao X, Fu J, Sheng G, Cui M, Li G (2003) Photoelectrocatalytic degradation of reactive brilliant orange K–R in a

new continuous flow photoelectrocatalytic reactor. Appl Catal A General 255:221–229
49. Zanoni MVB, Sene JJ, Anderson MA (2003) Photoelectrocatalytic degradation of remazol brilliant orange 3R on titanium dioxide thin-film electrodes. J Photochem Photobio A Chem 157:55–63